Articles

Solution Structure of the B-Myb DNA-Binding Domain: A Possible Role for Conformational Instability of the Protein in DNA Binding and Control of Gene Expression[†,‡]

Pauline B. McIntosh,[§] Tom A. Frenkiel,[||] Ute Wollborn,[⊥] John E. McCormick,[⊥] Karl-Heinz Klempnauer,[#] James Feeney,[⊥] and Mark D. Carr*[,§,@]

Laboratory of Molecular Structure, National Institute for Biological Standards and Control, Potters Bar, U.K., MRC Biomedical NMR Centre, National Institute for Medical Research, London, U.K., Division of Molecular Structure, National Institute for Medical Research, London, U.K., Hans-Spemann Laboratory, Max Planck Institut für Immunbiologie, Freiburg, Germany, and Department of Biosciences, University of Kent, Canterbury, U.K.

Received November 21, 1997; Revised Manuscript Received March 19, 1998

ABSTRACT: Double- and triple-resonance heteronuclear NMR spectroscopy have been used to determine the high-resolution solution structure of the minimal B-Myb DNA-binding domain (B-MybR2R3) and to characterize the specific complex formed with a synthetic DNA fragment corresponding to the Myb target site on the Myb-regulated gene *tom-1*. B-MybR2R3 is shown to consist of two independent protein domains (R2 and R3) joined by a short linker, which have strikingly different tertiary structures despite significant sequence similarities. In addition, the C-terminal region of B-Myb R2 is confirmed to have a poorly defined structure, reflecting the existence of multiple conformations in slow to intermediate exchange. This contrasts with the tertiary structure reported for c-MybR2R3, in which both R2 and R3 have the same fold and the C-terminal region of R2 forms a stable, well-defined helix [Ogata, K., et al. (1995) *Nat. Struct. Biol. 2*, 309−320]. The NMR data suggest there are extensive contacts between B-MybR2R3 and its DNA target site in the complex and are consistent with a significant conformational change in the protein on binding to DNA, with one possibility being the formation of a stable helix in the C-terminal region of R2. In addition, conformational heterogeneity identified in R2 of B-MybR2R3 bound to the tom-1-A target site may play an important role in the control of gene expression by Myb proteins.

The highly conserved mammalian and avian transcriptional control proteins c-Myb, A-Myb, and B-Myb play a central role in regulating the switch between the proliferation of progenitor cells and the initiation of differentiation. In particular, they appear to be involved in maintaining progenitor cells in a proliferative and nondifferentiated state, with down regulation of Myb expression accompanying differentiation (for reviews, see refs *1*−*6*). B-Myb is produced in virtually all cell lineages, and its expression is strictly dependent on cell proliferation (*7*, *8*). In contrast, c-Myb expression is mainly restricted to immature hematopoietic cells (*1*−*3*) and A-Myb expression to immature sperm cells, certain neuronal cell populations, B-lymphocytes, and breast ductal epithelium (*9*, *10*). The transcription of B-Myb is very tightly controlled during the cell cycle, reaching a peak in late G_1/S phase (*11*, *12*). Recently, the transcriptional activation potential of B-Myb has been shown to be regulated by cyclin-mediated phosphorylation, again consistent with B-Myb playing an important role in cell proliferation (*13*, *14*).

The Myb proteins contain a number of distinct functional domains, including an N-terminal DNA-binding domain, a central transactivation region, and a C-terminal regulatory domain (for reviews, see refs *1*−*6*). The Myb DNA-binding domain is composed of two or three imperfect repeats of approximately 52 amino acids (referred to as R1−R3;[1] *15*, *16*). In the case of B-Myb and c-Myb, the isolated R2R3

[†] This work was supported by the Medical Research Council (U.K.), the Department of Health (U.K.), and the Max-Planck Society (Germany). U.W. acknowledges the award of a postdoctoral fellowship from the Deutsche Forschungsgemeinschaft.

[‡] The coordinates of the 32 converged B-MybR2R3 structures, together with the experimental NMR constraints, have been deposited in the Brookhaven Protein Data Bank (PDB file names 1a5j and r1a5jmr, respectively).

* To whom correspondence should be addressed at Department of Biosciences, University of Kent, Canterbury, Kent CT2 7NJ, U.K.

[§] National Institute for Biological Standards and Control.

[||] MRC Biomedical NMR Centre, National Institute for Medical Research.

[⊥] Division of Molecular Structure, National Institute for Medical Research.

[#] Max Planck Institut für Immunbiologie.

[@] University of Kent.

[1] Abbreviations: B-MybR2R3, minimal B-Myb DNA-binding domain; c-MybR2R3, minimal c-Myb DNA-binding domain; R2, repeat 2 from the Myb DNA-binding domain; R3, repeat 3 from the Myb DNA-binding domain; 2D, two-dimensional; 3D, three-dimensional; NOE, nuclear Overhauser enhancement.

S0006-2960(97)02861-4 CCC: $15.00
Published on Web 06/18/1998

region has been shown to represent the minimal sequence-specific DNA-binding domain (*15*, *17*−*19*). The role of R1 is unclear; however, it may be involved in mediating important interactions with other transcriptional control proteins or play a more general role in stabilizing specific protein−DNA complexes (*20*).

The Myb transcription factors have been shown to bind to DNA target sites as monomers (*17*), and both B-Myb and c-Myb were found to recognize a core 6 base pair site with the consensus sequence PyAACG/TG ($K_d \sim 1-3$ nM; *16*, *19*, *21*). To date, several bona fide Myb-regulated genes have been identified, including *mim-1* and *tom-1*, which both contain essential Myb target sites in their promoter regions (*5*, *22*, *23*).

Some insight into the structural organization and properties of Myb DNA-binding domains has been provided by our own NMR work on B-MybR2R3 (*24*) and by two parallel studies of c-MybR2R3 (*25*−*27*). For example, we recently reported that the minimal B-Myb DNA-binding domain contains three stable helices in R3 but only two in R2. The C-terminal region of R2, which is believed to form one-half of the DNA-binding site and corresponds to the third helix in R3, was found to exist in multiple conformations in solution and was found to form a so-called unstable helix (*24*, *28*). This conformational instability in part of the DNA-binding motif of B-Myb was proposed to increase the specificity of Myb proteins for a relatively short (6 base pairs) DNA target site by reducing their affinity for nonspecific DNA sequences compared to that for specific sites (*24*). A very similar secondary structure to B-MybR2R3 was found for c-MybR2R3 by Jamin et al. (*25*); however, a second NMR study of c-MybR2R3 reported that both R2 and R3 contain three stable helices and have near identical tertiary structures (*26*, *27*), which is obviously inconsistent with the other two NMR studies of minimal Myb DNA-binding domains.

In this paper, we report the determination of a high-resolution solution structure for the minimal B-Myb DNA-binding domain (B-MybR2R3), which confirms the differences in the secondary structures of the two repeats reported previously (*24*). This study clearly shows that R2 and R3 from B-Myb have strikingly different tertiary structures despite significant sequence similarities. We have also used a specific Myb DNA target site to probe the protein surfaces involved in interactions with DNA; the NMR data suggest there are extensive contacts between B-MybR2R3 and its DNA target site and are consistent with conformational changes in the protein on DNA binding. In addition, a number of protein residues in DNA-bound B-MybR2R3 give rise to two sets of NMR signals, an indication of the presence of two forms of the B-MybR2R3−DNA complex.

EXPERIMENTAL PROCEDURES

Sample Preparation. The expression and purification of nonisotopically enriched and uniformly ^{15}N- or ^{15}N- and ^{13}C-labeled B-MybR2R3 were carried out as described previously (*24*). A 16-base deoxynucleotide with the sequence TCCTTAACGGACTGAG and its complementary strand were obtained as HPLC-purified products from Oswell. To prepare the double-stranded 16-mer corresponding to the B-Myb target site in the tom-1-A promoter of the *tom-1* gene, equal amounts (1.3 μmol) of the two complementary deoxynucleotides were mixed at room temperature in 0.86 mL of 25 mM potassium phosphate, 100 mM potassium chloride, and 100 μM EDTA (pH 6.0) buffer and then annealed by cooling slowly from 80 °C. The B-MybR2R3−tom-1-A 16-mer complex was formed by adding a 0.6 mL solution of the tom-1-A 16-mer to 0.76 μmol of freeze-dried ^{15}N-labeled B-MybR2R3. The complex was then freeze-dried and collected in 0.6 mL of 90% H_2O/10% D_2O to give a 1.3 mM NMR sample.

NMR Measurements. The NMR experiments were carried out at 15 °C on Varian Unity spectrometers operating at 500 and 600 MHz using 0.6 mL samples of 2.0−3.5 mM unlabeled, 0.9 mM ^{15}N- and ^{13}C-labeled, and 1.3−2.9 mM ^{15}N-labeled B-MybR2R3 or B-MybR2R3 bound to the tom-1-A DNA target site, which were dissolved in a 25 mM potassium phosphate, 100 mM potassium chloride, and 50 μM EDTA (pH 6.0) buffer. A detailed description of the many single-, double-, and triple-resonance experiments used to obtain essentially complete sequence-specific ^{15}N, ^{13}C, and ^{1}H resonance assignments for B-MybR2R3 is given in Carr et al. (*24*). In addition, 3D ^{15}N/^{1}H HNHA (*29*), HNHB (*30*), and ROESY−HMQC (*31*) spectra were recorded from ^{15}N-labeled B-MybR2R3. A continuous wave spin-lock field of 3 kHz for 25 ms was used in the ROESY−HMQC experiment. In the case of the B-MybR2R3−tom-1-A 16-mer complex, a 3D ^{15}N/^{1}H NOESY−HSQC (*32*) spectrum was acquired over 64 h with an NOE mixing time of 50 ms and acquisition times of 17 (F_1), 10 (F_2), and 64 ms (F_3). Slowly exchanging amide protons in B-MybR2R3 were identified from a series of 2D ^{15}N/^{1}H HMQC (*33*) spectra recorded over 12 h from a sample of ^{15}N-labeled protein freshly dissolved in D_2O. For the HMQC and ROESY−HMQC spectra, water supression was realized by using selective presaturation at the water frequency; however, for the HNHA, HNHB, and NOESY−HSQC experiments, the pulsed-field gradient-based WATERGATE method was used (*34*).

The NMR data were processed on SUN workstations using the Varian VNMR software package for 2D spectra and software written at the MRC Biomedical Centre for 3D experiments (C. J. Bauer, unpublished work). To improve the resolution in the HNHB, HNHA, and ROESY−HMQC spectra, linear prediction (*35*) was used to increase the effective acquisition times from 15 to 22 ms in the ^{15}N dimension and from 19 to 29 ms in the indirect ^{1}H dimension. Similarly, the effective acquisition times for the NOESY−HSQC experiment on the complex were increased from 10 to 15 ms in the ^{15}N dimension and from 17 to 25 ms in the indirect ^{1}H dimension. In addition, the time domain matrices were zero-filled at least once in all dimensions, and mild resolution enhancement was realized by applying a π/2.5-shifted sine-squared apodization function in all dimensions. All the spectra were analyzed on-screen using the program XEASY (*36*).

Structural Calculations. Structurally significant intraresidue and interresidue NOEs were identified from 3D ^{15}N/^{1}H NOESY−HMQC, 3D ^{13}C/^{1}H HMQC−NOESY, and 2D NOESY spectra of B-MybR2R3 recorded with mixing times of 70 (5 °C) or 100 ms (15 °C), as described previously (*24*). The relationship between NOE intensity and interproton distance was calibrated using NOEs corresponding to

known distances in regular α-helical regions of B-MybR2R3 [NH−$NH_{(i,i+1)}$, αCH−$NH_{(i,i+3)}$, etc.], and on this basis, the NOEs were converted to upper distance constraints of 2.8, 3.3, 4.0, 5.0, or 6.0 Å. Where appropriate, standard distance corrections were applied to constraints involving methyl and aromatic ring protons (*37*). In addition, a further correction of 0.5 Å per group involved was added to distance constraints involving methyl, tryptophan HD1, and histidine HD2 and HE1 atoms to compensate for the higher apparent intensity of NOEs involving these sharp signals.

The ratios of diagonal to cross-peak volumes from the HNHA spectrum allowed the determination of reliable $^3J_{NH-\alpha CH}$ coupling constants (±1, 1.5, or 2 Hz) for 93 residues in B-MybR2R3. Similarly, the relative intensities of NH−αCH cross-peaks in the HNHB spectrum identified 49 residues in B-MybR2R3 for which the $^3J_{N-\alpha CH}$ coupling constants could be assigned as either large (−5 ± 0.5 Hz) or small (−1 ± 0.5 Hz). This coupling constant data was used as input for the program HABAS (*38*), which produced constraints for 82 ϕ and 82 φ torsion angles in B-MybR2R3.

Initially, a family of 50 structures were calculated for B-MybR2R3 from random starting coordinates using the redundant dihedral angle constraint (REDAC) protocol implemented in the distance geometry program DIANA (*38*, *39*). These calculations were based on 1189 upper distance limits (537 intraresidue and 652 interresidue) and 164 ϕ and φ torsion angle constraints. As part of the refinement process, new generations of B-MybR2R3 structures were then recalculated from random starting coordinates using the additional structural information generated at each of the following stages. (i) The initial converged B-MybR2R3 structures, together with the $^3J_{N-\alpha CH}$ coupling constant and NH−αCH ROE data, were used to determine stereospecific assignments and χ^1 angle ranges for 16 β-methylene and five valine γ-methyl groups, as well as χ^1 values for two threonine and five isoleucine residues. The χ^1 angle constraints were included in the structural calculations with ranges of ±30°. (ii) In the next step, the second-generation converged B-MybR2R3 structures were used in the program ASNO (*40*) to assign a further 199 interresidue NOEs, which were ambiguous with chemical shift information only. (iii) Finally, analysis of the third-generation B-MybR2R3 structures and appropriate NOE-derived distance constraints with the molecular graphics package MOLMOL (*41*) allowed the determination of nine additional stereospecific assignments for six β-methylene, one γ-methyl, and three δ-methyl groups. In addition, for both phenylalanine 71 and tyrosine 25, which have well defined χ^1 angles, it was possible to assign many NOEs involving degenerate HD1/HD2 or HE1/HE2 aromatic signals to one side of the aromatic ring.

In the final stages of the structure refinement, 84 additional distance constraints were included in the calculations corresponding to 21 NMR-determined backbone hydrogen bonds. The hydrogen bonds were only imposed for residues located in either regular α- or 3_{10}-helices and for which the amide proton involved was detectable after at least 30 min in D_2O. For each hydrogen bond, appropriate lower and upper distance limits were used to constrain NH−O to 1.8−2.3 Å and N−O to 2.4−3.3 Å.

The final B-MybR2R3 structures were calculated with the new program DYANA (*42*), which uses simulated annealing combined with restrained molecular dynamics in torsion angle space to generate protein structures consistent with NMR data. A total of 100 structures were calculated from random starting conformations using a simulated annealing protocol consisting of 3000 molecular dynamics steps at high temperatures followed by slow cooling over 12 000 steps, with a short conjugate gradient minimization at the end. In addition, three cycles of the REDAC procedure were included in the calculations to maximize the number of converged B-MybR2R3 structures obtained.

Analysis of the structures of the B-Myb and c-Myb DNA-binding domains (rmsd values, Ramachandran plots, angular order parameters, solvent accessibilities of residues, interhelical angles, etc.) was carried out using the programs MOLMOL (*41*) and DYANA (*42*). In addition, MOLMOL was used to prepare all the protein structure figures.

RESULTS AND DISCUSSION

Solution Structure of the B-Myb DNA-Binding Domain. The high-resolution solution structure of the minimal B-Myb DNA-binding domain (B-MybR2R3) was determined using a total of 1685 NMR-derived structural constraints (an average of 15.3 per residue), including 1402 NOE-based upper distance limits [538 intraresidue, 311 sequential ($i - j = 1$), 338 medium-range ($1 < i - j \leq 4$), and 215 long-range ($i - j > 4$); Figure 1], 84 hydrogen bonding constraints, and 199 dihedral angle constraints (82 ϕ, 82 φ, and 35 χ^1). As a result of the final DYANA calculations (*42*), 32 satisfactorily converged B-MybR2R3 structures were obtained from the 100 random starting conformations. The converged structures contain no distance constraint or van der Waals violations greater than 0.5 Å and no dihedral angle constraint violations over 6° and have an average target function of 8.22 ± 1.11. The sums of the violations for upper distance limits, lower distance limits, van der Waals contacts, and torsion angle constraints were 29.7 ± 1.83 Å, 0.47 ± 0.16 Å, 11.82 ± 1.49 Å, and 30.96 ± 7.23°, respectively. Similarly, maximum violations for the converged structures were 0.46 ± 0.03 Å, 0.17 ± 0.07 Å, 0.32 ± 0.07 Å, and 4.68 ± 0.95°, respectively.

The B-MybR2R3 structures all show good nonbonded contacts, as illustrated by the Ramachandran plot shown in Figure 2a. Typically, there are only one or two residues per structure (an average of 1.62 ± 1.13) with combinations of φ and ψ that lie outside of the favored regions and no residues that consistently adopt less favorable backbone conformations. In addition, all the residues that occasionally show less favorable combinations of φ and ψ have low angular order parameters (<0.9) for one or both of these backbone dihedral angles (Figure 2b).

In the case of B-MybR2R3, no NOEs were detected between R2 and R3 and only a few nonsequential NOEs were identified in the region linking the two domains (L53−S61), as illustrated in Figure 1. In addition, residues in the linker (L53−S61) have low angular order parameters for both φ and ψ (Figure 2b). Thus, the minimal B-Myb DNA-binding region would appear to consist of two independent protein domains (R2 and R3) joined by a flexible linker of six to eight residues. The distinct backbone topologies of the two domains are illustrated in Figure 3, which shows the best-fit superpositions of the protein backbone for both

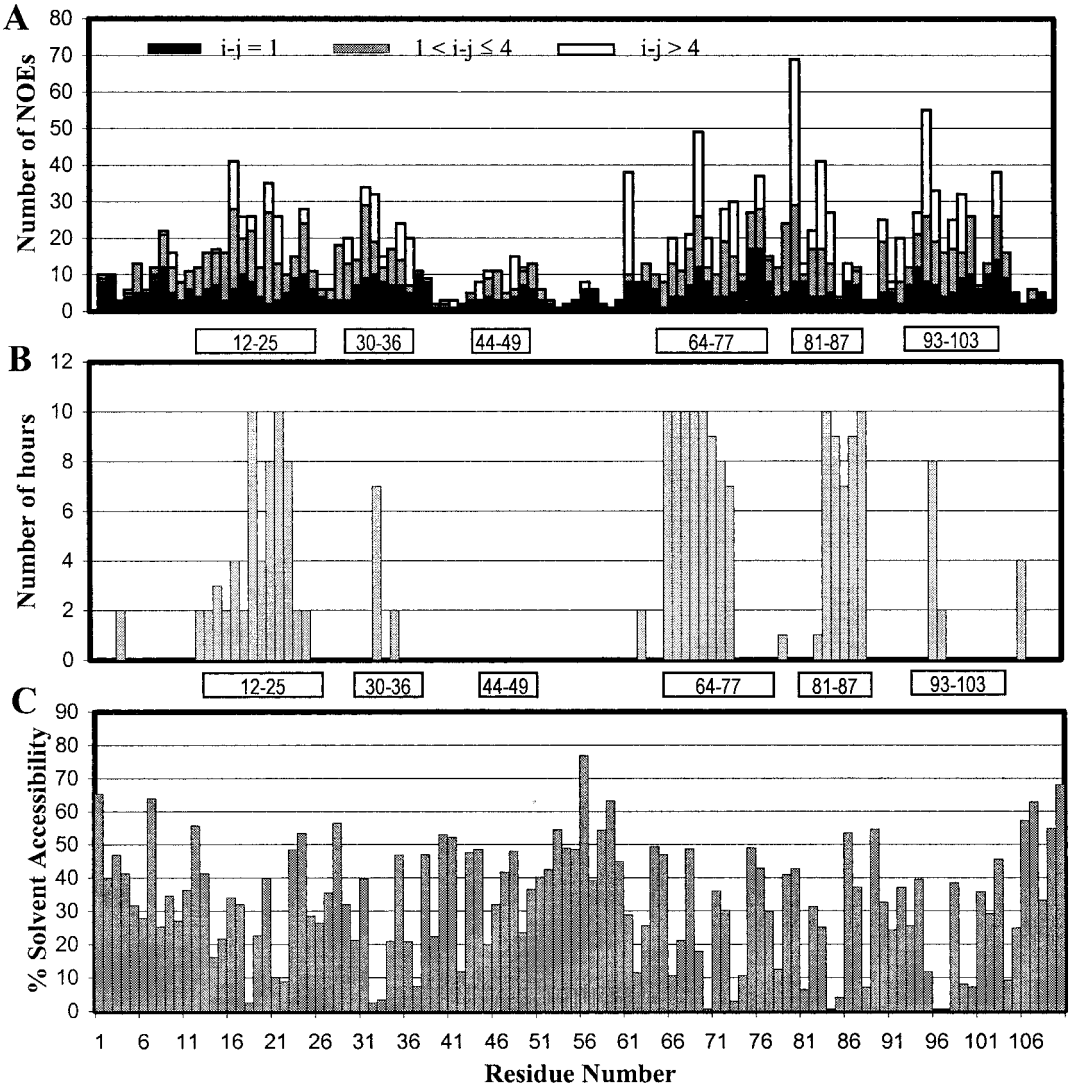

FIGURE 1: Summary of the interresidue NOE, backbone amide exchange, and solvent accessibility data obtained for B-MybR2R3. The locations of the five regular helices and the unstable helix identified are indicated between the plots. (A) A histogram showing the sequential ($i - j = 1$), medium-range ($1 < i - j \leq 4$), and long-range ($i - j > 4$) interresidue NOEs identified for B-MybR2R3. (B) An illustration of the length of time that backbone amide protons of B-MybR2R3 persist in D_2O, with slowly exchanging amide protons localized to areas of helical structure. (C) A histogram showing the calculated solvent accessible surface area of each residue in the structures determined for B-MybR2R3. The values reported are expressed as a percentage of the accessible area of the isolated residue.

R2 and R3 calculated from the family of 32 converged structures obtained for B-MybR2R3.

R2 from B-Myb folds into a relatively flat and elongated protein domain with a well-defined core (W10−K38) composed of two α-helices (K12−Y25 and W30−H36) connected by a short loop, which collectively form a hairpin-like structure (Figure 3). The poorly defined C-terminal region (G42−W49) lies across one face of the hairpin (Figure 3), with its orientation determined by a number of long-range NOEs to residues in the helix−loop−helix region (I19−W49, V22−W49, W30−C45, W30−R46, I33−C45, A34−L41, and A34−A42). The N (G1−P9)- and C (H50−N54)-terminal residues of R2 are disordered (Figures 2b and 3). The hairpin-like structure is stabilized by a small, well-defined hydrophobic core, involving the side chains of residues V18, V22, L32, I33, and L37 (Figure 4), which is reflected in the low solvent accessibility of these residues (Figure 1). The side chains of W30, C45, R46, and W49 are also significantly shielded from solvent and form the main contact surface between the C-terminal region and the hairpin. The relative orientation of the two α-helices in R2 is very well-defined, which is reflected in a root-mean-square deviation (rmsd) of the backbone atom coordinates (N, C_α, and C) for the helical residues of 0.51 ± 0.13 Å for the family of converged B-MybR2R3 structures. A similarly high level of precision is obtained for the complete hairpin region of R2 (Table 1), but rmsd values rise significantly (>1.2 Å) when residues G39−N51 are also included. As expected, the precision to which regions of R2 have been determined shows a strong correlation with the number of interresidue NOEs observed (Figure 1).

Recently, we reported clear and unambiguous chemical shift, line broadening, and NOE evidence for the existence of multiple conformations in the C-terminal region of R2 from B-MybR2R3 (L41−L53), in slow to intermediate exchange on the NMR time scale at 15 °C (*24*). A number of conformational exchange processes could result in the observed line broadening of resonances; however, the NMR data as a whole appear to indicate that residues Q44−W49 exist in several interconverting states in solution but adopt

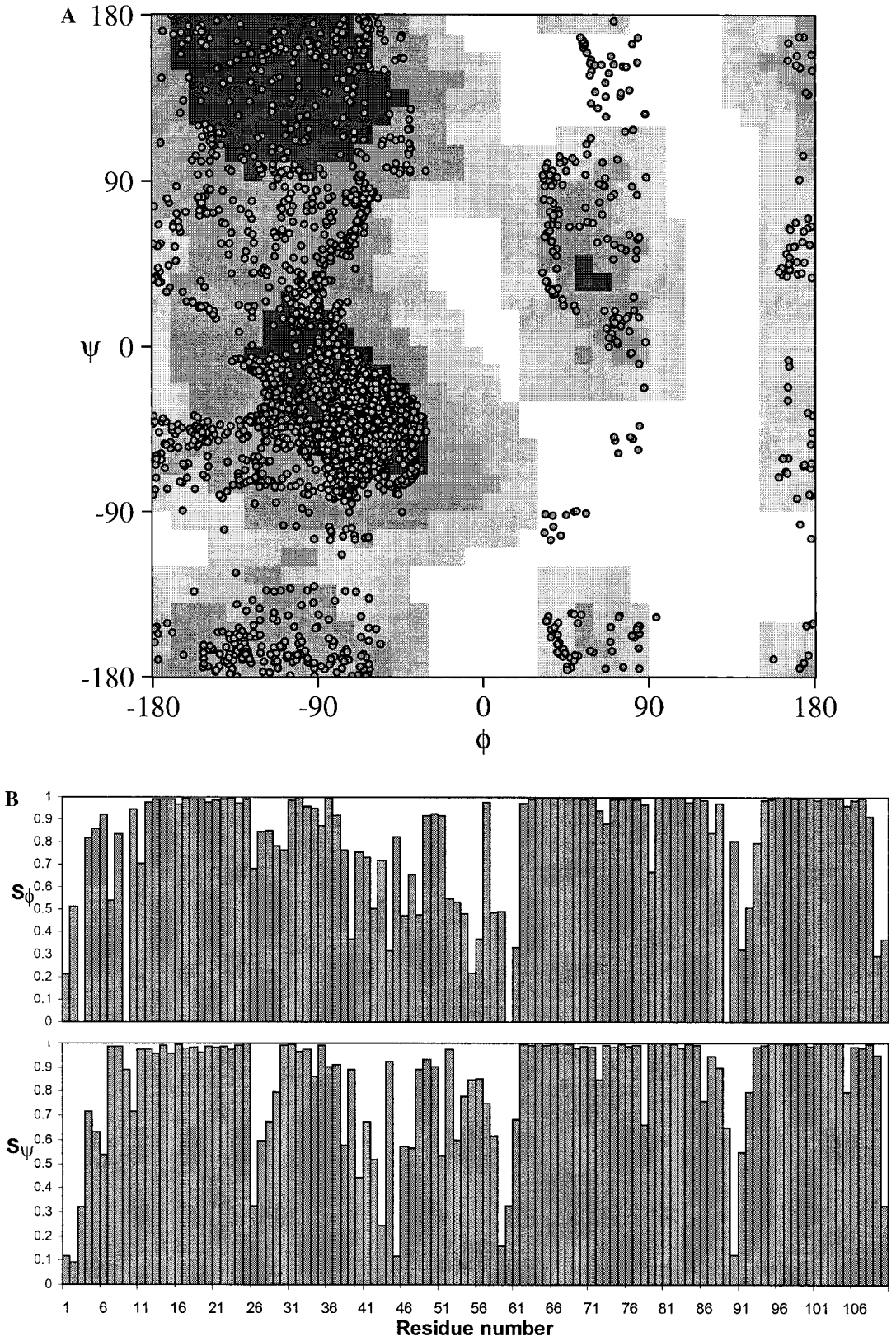

FIGURE 2: Distribution and precision of backbone dihedral angles in the family of 32 converged B-MybR2R3 structures. (A) A Ramachandran plot showing the distribution of φ and ψ angles for all non-glycine and non-proline residues in the 32 B-MybR2R3 structures. (B) Angular order parameters for the backbone φ and ψ dihedral angles in the converged B-MybR2R3 structures.

local helical or turn-like conformations for a significant fraction of the time and therefore form a so-called unstable helix. The relatively poorly defined structure for the C-terminal region of R2 almost certainly reflects this conformational heterogeneity, which in turn accounts for the observation of fewer NOEs involving this area of R2. The presence of an unstable helix near the C terminus of R2 is actually reflected in a number of the structures determined for B-MybR2R3, which contain short stretches (three or four residues) of α- or 3_{10}-helix distributed evenly over residues

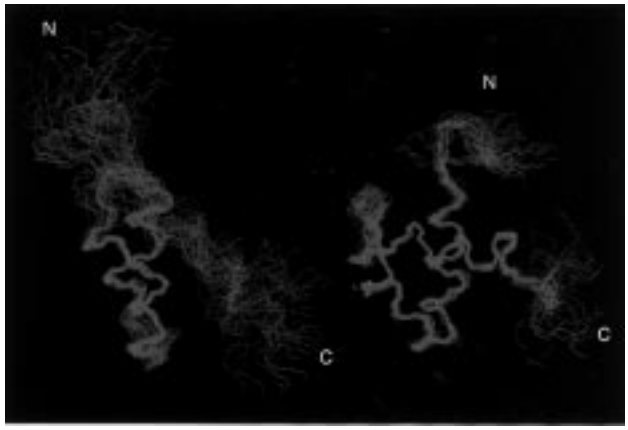

FIGURE 3: Best-fit superposition of the protein backbone for the 32 converged structures obtained for B-MybR2 (residues 1−54 and shown on the left) and B-MybR3 (residues 55−110). The structures were superimposed on residues 12−25 and 30−36 for R2 and on residues 64−77, 81−87, and 93−103 for R3.

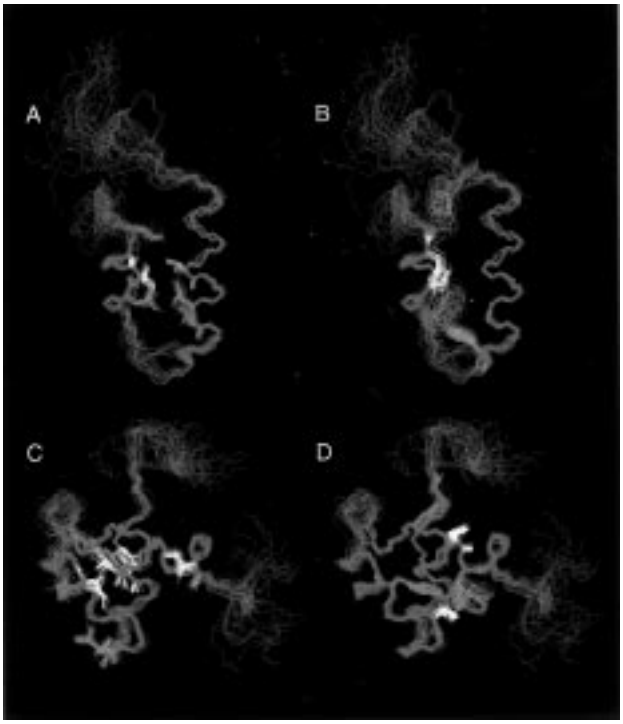

FIGURE 4: Comparison of the hydrophobic cores in R2 and R3 of B-Myb. Structures were superimposed on residues 12−25 and 30−36 for R2 and on residues 64−77, 81−87, and 93−103 for R3. The protein backbone is shown in magenta, and the side chains of leucine and tryptophan are shown in green, isoleucine and histidine in yellow, and valine, phenylalanine, and tyrosine in red. (A) Hydrophobic aliphatic residues of R2 (L21, L32, L37, I33, V18, and V22). (B) Aromatic residues of R2 (W10, W30, Y25, and H36). (C) Hydrophobic aliphatic residues of R3 (L77, L87, L88, I69, I70, I84, I104, V76, and V96). (D) Aromatic residues of R3 (W62, W100, W81, F71, H74, and H99).

43−53 (Figure 2).

In contrast to R2, R3 in B-MybR2R3 forms a compact globular domain composed of three stable α-helices (E64−L77, W81−L87, and D93−T103) connected by short loops (Figure 3), which form a well-defined core (W62−K105). As in R2, the N (P55−S61)- and C (D109−T110)-terminal residues are disordered (Figures 2b and 3). The structure of R3 is stabilized by hydrophobic interactions between a number of conserved residues, all of which have characteristically low solvent accessibilities and show a large number of long-range NOEs (Figure 1). Residues I69, I70, I84, A85, L88, and V96 form the basis of the hydrophobic core, while interactions between the aromatic rings of H74, W81, and W100 anchor the C terminus of helix 1 and the N terminus of helix 2 to helix 3. Similarly, the aromatic ring of W62 stacks on the ring of H99 to anchor the N terminus of helix 1 to helix 3 (Figure 4). The solution structure of B-Myb R3 is determined to very high precision, which is reflected in the low rmsd values for both backbone and side chain coordinates given in Table 1. For example, backbone atoms in the three helices show an rmsd from the mean of only 0.34 ± 0.07 Å for the family of 32 converged structures.

Table 1: (A) Root-Mean-Square Deviations for the 32 Converged Structures Obtained for B-MybR2R3 Compared to the Mean Coordinates[a] and (B) All Pairwise Root-Mean-Square Deviations between Equivalent Regions of the NMR-Derived Structures of the Repeats (R2 and R3) in B-MybR2R3 and c-MybR2R3[b]

A	rmsd ± standard deviation (Å)	
	backbone atoms	all heavy atoms
R2 helices (K12−Y25 and W30−H36)	0.51 ± 0.13	1.05 ± 0.17
R2 structured residues (W10−K38)	0.74 ± 0.16	1.41 ± 0.25
R3 helices (E64−L77, W81−L87, and D93−T103)	0.34 ± 0.07	0.75 ± 0.12
R3 structured residues (W62−K105)	0.44 ± 0.09	0.87 ± 0.12

B	B-Myb R2/R3	c-Myb R2/R3	R2 B-Myb/ c-Myb	R3 B-Myb/ c-Myb
helix 1 + helix 2	1.31 ± 0.15	0.64 ± 0.11	1.45 ± 0.16	1.02 ± 0.17
helix 1 + helix 2 + helix 3	2.42 ± 0.38	0.73 ± 0.09	2.30 ± 0.36	1.03 ± 0.14

[a] Values are quoted for the superposition of several subsets of residues in B-MybR2R3. [b] The values given are based on the superposition of equivalent residues from the three helical regions in the repeats. The residues included for helix 1 were 12−25 (B-MybR2), 64−77 (B-MybR3), 97−110 (c-MybR2), and 149−162 (c-MybR3), for helix 2 were 30−36 (B-MybR2), 81−87 (B-MybR3), 115−121 (c-MybR2), and 166−172 (c-MybR3), and for helix 3 were 42−51 (B-MybR2), 93−102 (B-MybR3), 127−136 (c-MybR2), and 178−187 (c-MybR3).

Structural Homology between R2 and R3 from B-Myb. The two N-terminal helices in R2 and R3 occupy essentially identical positions in the two domains, consistent with the high degree of amino acid sequence similarity between these regions in R2 and R3 (65%). The structures of the equivalent helices are also very similar, with best-fit superpositions of the backbone atoms for helix 1 and helix 2 from both domains giving all pairwise rmsd values of 0.73 ± 0.17 and 0.80 ± 0.16 Å, respectively. In contrast, the C-terminal region forming the third helix in R3 (D93−T103) shows very little sequence conservation between R2 and R3 (<20%), and the local conformations differ significantly, as reported previously (*24*), which is reflected in an all pairwise rmsd of 2.33 ± 0.26 Å for the backbone atom coordinates of residues G42−H52 from R2 compared to that for helix 3 in R3.

Although the two N-terminal helices in B-Myb R2 and R3 are structurally very similar, Figures 3 and 4 clearly illustrate that there is a striking difference in the orientation of the helices with respect to each other in R2 and R3, and therefore in the tertiary structures of the two domains. The angle between helix 1 and helix 2 in R2 is 21.0 ± 6.5°, while the corresponding angle in R3 is considerably larger at 35.8

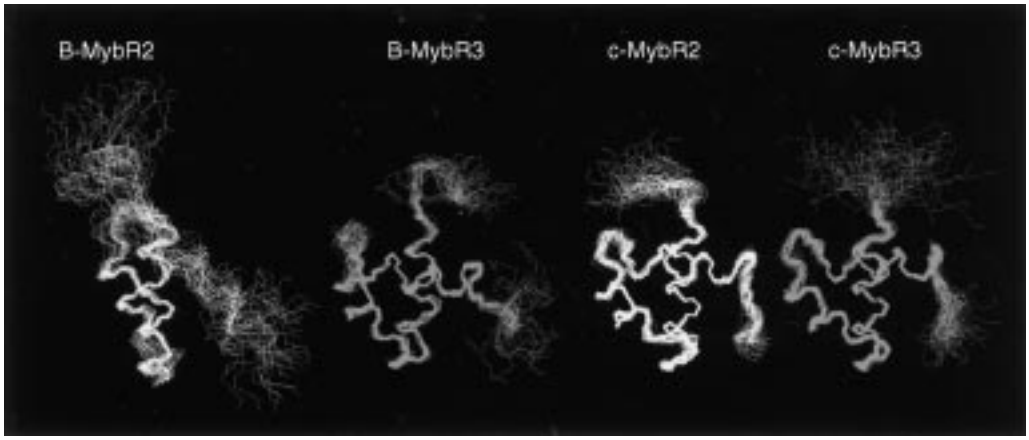

	B-MybR2		B-MybR3		c-MybR2		c-MybR3	
	Helix-2	Nascent Helix	Helix-2	Helix-3	Helix-2	Helix-3	Helix-2	Helix-3
Helix-1	21.0+/-6.5	56.4+/-10.9	35.8+/-3.3	83.9+/-6.2	42.1+/-1.9	90.6+/-2.0	41.9+/-4.2	95.8+/-3.8
Helix-2		45.5+/-11.2		74.7+/-4.2		71.9+/-2.2		66.9+/-4.1

FIGURE 5: Comparison of the solution structures determined for R2 and R3 from B-Myb with those reported for c-Myb, which highlights the striking differences in the structures of R2 from B-Myb and c-Myb. (A, top) Families of converged structures obtained for R2 and R3 from both B-Myb and c-Myb (1mbh and 1mbk) with helix 1 shown in exactly the same orientation for all structures. (B, bottom) The values determined for interhelical angles in B-Myb and c-Myb.

± 3.3°. Similarly, there are large differences between R2 and R3 in the orientation of the C-terminal region forming the third helix in R3 with respect to the N-terminal helices (Figures 3 and 5). For example, the interhelical angle between helix 1 and this region is 56.4 ± 10.9° in R2 but 83.9 ± 6.2° in R3. Clearly, these large differences in the relative orientations of the helices in R2 and R3 reflect the significantly different tertiary structures of the two domains. In effect, the backbone topology of R2 from B-Myb can be considered a flattened R3 fold (Figures 3 and 5).

A comparison of the amino acid sequences of R2 and R3 from B-Myb reveals that 17 of the 52 positions are occupied by identical residues and a further seven by conservative substitutions. However, there are important sequence differences between the two repeats, some of which may account for the very distinct tertiary structures of R2 and R3. In R3, the side chains of H74 and H99 make critical interactions with the aromatic rings of the strictly conserved tryptophan residues, which serve to anchor helix 3 to both ends of helix 1 (W62−H99 and H74−W100) and also the C terminus of helix 1 to the N terminus of helix 2 (H74−W81), as illustrated in Figure 4. These histidine residues are strictly conserved in all mammalian and avian R3 sequences (c-Myb, A-Myb, and B-Myb) but are not present in R2, where H74 is substituted by lysine (B-Myb) or glutamine (c-Myb and A-Myb) and H99 by arginine (A-Myb, B-Myb, and c-Myb). The absence of these structurally important interactions between histidine and tryptophan rings in R2 almost certainly accounts for the striking differences in the tertiary structures of B-Myb R2 and R3 and could also result in the conformational heterogeneity at the C terminus of R2.

On the basis of the solution structure determined for c-MybR2R3, Ogata and co-workers proposed that cavities in the hydrophobic core of c-Myb R2 could account for the reduced stability of R2 compared to that of R3 (*27*). The structure of the hydrophobic core in B-Myb R2 is very different from that reported for c-Myb R2, reflecting the strikingly different tertiary structure, and so the explanation proposed for the reduced stability of c-Myb R2 is not applicable to the conformational heterogeneity identified in B-Myb R2.

The rates at which backbone amide protons exchange with water can provide useful information on the relative stability of regions of a protein. In R2 of B-Myb, all the slowly exchanging backbone amide protons are localized in the two N-terminal helices. Similarly, they are mainly confined to the helical regions in R3, but the percentage of slowly exchanging amide protons is significantly lower in helix 3 than in either helix 1 or helix 2 (Figure 1). This data not only confirms the instability observed in the C-terminal region of B-Myb R2 (*24*) but also suggests a somewhat reduced stability in the third helix of R3.

Comparison of the B-Myb and c-Myb DNA-Binding Domains. The minimal DNA-binding domains (R2R3) from B-Myb and c-Myb have a very high level of amino acid sequence homology (85% identity and 10% conservative substitution), which should be reflected in very similar secondary and tertiary structures for the domains. Two independent groups have recently reported NMR-based structural studies of c-MybR2R3 proteins similar in size to B-MybR2R3. In the first report, Jamin et al. (*25*) showed that a 105-residue c-MybR2R3 protein contained two helices in R2 and three helices in R3, involving amino acids corresponding to K12−Y25, W30−H36, E64−L77, R80−L87, and D93−S102 in B-MybR2R3. They were unable to obtain sequence-specific resonance assignments for the last 13 C-terminal residues of R2, due to missing or very weak NMR correlations to the amide protons, and proposed that this region exists in several distinct conformations at 10−20 °C and pH 6.6 (*25*). More recently, Ogata and co-workers (*26*, *27*) studying a 104-residue c-MybR2R3 protein have

confirmed the five helical regions identified previously. However, in contrast to the work of Jamin et al. (*25*), they reported that residues in the C-terminal region of c-Myb R2 (corresponding to amino acids G42−N51 in B-Myb) form a stable helix at 17−27 °C and pH 6.8, equivalent in both length and position to the third helix in c-Myb R3. The two groups have studied nearly identical proteins under very similar conditions, so it is very difficult to account for the reported differences in the secondary structure of c-Myb R2. As reported previously (*24*), the secondary structure determined for B-MybR2R3 is essentially identical to that proposed for c-MybR2R3 by Jamin et al. (*25*) and the C-terminal region of B-Myb R2 has also been shown to be conformationally unstable, with residues Q44−W49 forming an unstable helix.

The high-resolution solution structures for R2 and R3 from both B-Myb and c-Myb (*26*, *27*) are shown in identical orientations in Figure 5. The tertiary structures of R3 from B-Myb and c-Myb are very similar, which is reflected in an all pairwise rmsd of 1.03 ± 0.14 Å for the backbone atoms of the three helices and in similar interhelical angles (Figure 5). In contrast, the solution structure reported by Ogata et al. (*26*, *27*) for R2 from c-Myb is strikingly different from that determined for B-Myb R2 (Figure 5 and Table 1). As discussed previously, significant amino acid sequence differences between R2 and R3 in vertebrate Myb proteins (A-Myb, B-Myb, and c-Myb) could account for the distinct secondary and tertiary structures obtained for the two repeats of B-Myb and for similar secondary structural differences reported by Jamin et al. (*25*) for c-MybR2R3. In the case of R2, the structure of Ogata and co-workers for c-Myb is clearly not compatible with that determined by Jamin et al. (*25*) and is very different from that reported here for B-Myb R2.

Identification of the DNA-Binding Site on B-MybR2R3. Comparison of the $^{15}N/^{1}H$ HSQC spectra obtained for free and DNA-bound B-MybR2R3 (Figure 6) reveals dramatic changes in the backbone amide ($^{15}N/^{1}H$) chemical shifts of many residues in the protein on complex formation, suggesting a large contact surface with the DNA and/or significant conformational changes in B-MybR2R3 on DNA binding. Sequence-specific ^{15}N and ^{1}H resonance assignments for the backbone amide signals of B-MybR2R3 in its complex with the *tom-1* DNA target site were obtained by analysis of the 3D $^{15}N/^{1}H$ NOESY−HSQC spectrum. Initially, patterns of NOEs involving amide protons, together with amide ^{15}N and ^{1}H chemical shifts in the complex, were compared to those of the free protein to identify those residues that showed no significant changes in these parameters on DNA binding. Subsequently, NH−NH NOEs were used to confirm these assignments and to identify neighboring residues in the sequence, thereby building up stretches of assigned amide signals for B-MybR2R3 in the complex. This strategy proved successful and allowed assignments to be made for 79 of the 105 backbone NH groups in the protein and for 8 of the 14 side chain NH_2 signals. Signals corresponding to probably all of the remaining backbone amide groups of bound B-MybR2R3 were observed in the $^{15}N/^{1}H$ spectra of the complex but could not be assigned due to a combination of spectral overlap and NOE and chemical shift patterns that differed significantly from those of the free protein. The majority of the residues for which the backbone amide signals could not be assigned were located in the C-terminal regions of R2 and R3.

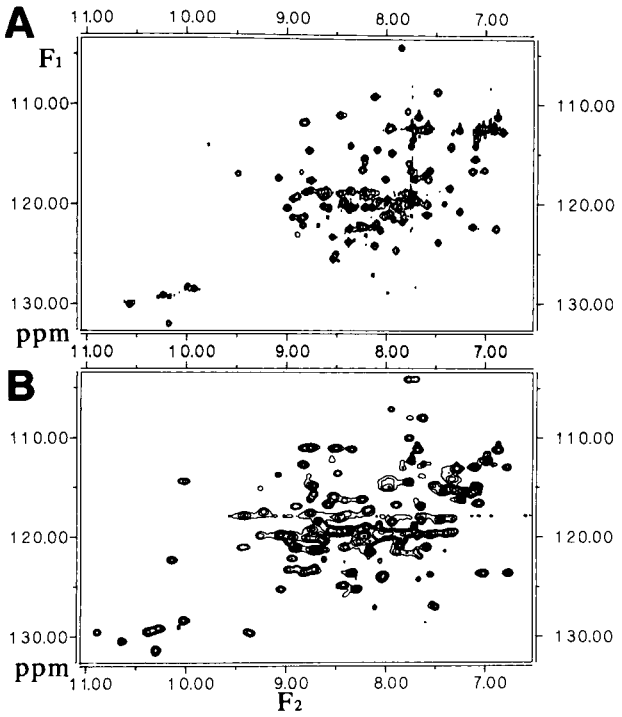

FIGURE 6: $^{15}N/^{1}H$ HSQC spectra of free B-MybR2R3 (A) and in a complex (B) with a specific DNA target site (tom-1-A 16-mer). The spectra illustrate the large backbone amide chemical shift changes induced in B-MybR2R3 on binding to DNA.

For residues in B-MybR2R3 whose amide signals were not assigned in the complex, lower limits for the changes in chemical shifts of the backbone amide signals (^{1}H and ^{15}N) induced on binding to the DNA target site were determined by measuring the cumulative chemical shift changes to the nearest backbone amide cross-peaks in HSQC spectra of the complex (*43*). The nearest cross-peaks were determined by considering both the ^{1}H and ^{15}N chemical shift changes, with the ^{15}N shift scaled for the difference in the spectral dispersion of the backbone amide ^{15}N resonances compared to the ^{1}H signals to give a roughly equal weight to each. Thus, by calculation of the sums of the magnitudes of the changes in ^{1}H and scaled ^{15}N chemical shifts, the nearest backbone amide cross-peaks in the complex were determined as those with the lowest cumulative chemical shift changes ($\sum\delta = |\delta^{1}H| + |\delta^{15}N/7.1|$ or $|\delta^{1}H| + |\delta^{15}N/1.8|$ for glycines; *43*).

Measurement of chemical shift perturbations on complex formation is well-established as a useful probe of ligand binding sites on proteins, and Figure 7 summarizes the pattern of backbone amide chemical shift changes observed for B-MybR2R3 on binding to the tom-1-A DNA target site. In general, similar patterns of chemical shift changes are observed for equivalent regions of R2 and R3, but with somewhat larger shifts seen for some residues in R3. The data show that no significant shifts in backbone amide signals occur for residues in the first helix of both repeats but large changes are seen for amino acids located in the second helix of R2 and R3. Significant spectral changes are also observed for residues at both the N (E56−S61) and C termini (N101−V108) of R3 and the N terminus (L5−W10) of R2. The changes in backbone amide chemical shifts for residues in

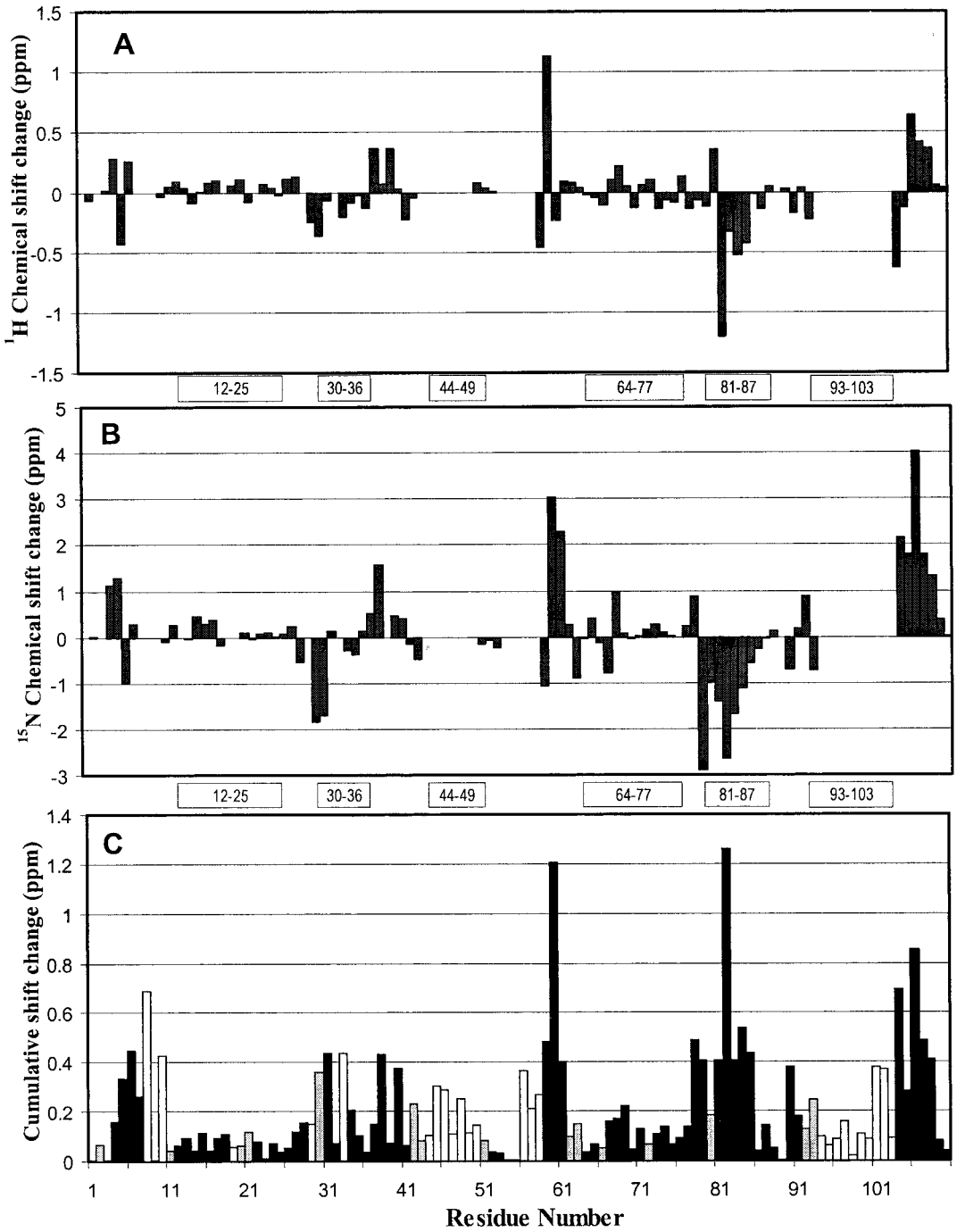

FIGURE 7: Summary of the backbone amide chemical shift changes observed on binding of B-MybR2R3 to a specific DNA target site. The five helices and so-called unstable helix identified in the free protein are indicated between the plots: (A) changes in backbone amide proton chemical shift, (B) changes in backbone nitrogen chemical shift, and (C) the change in the cumulative chemical shift ($\sum\delta = |\delta^1\text{H}| + |\delta^{15}\text{N}/7.1|$ or $|\delta^1\text{H}| + |\delta^{15}\text{N}/1.8|$ for glycines). Assignments for backbone amide signals of B-MybR2R3 in the complex were obtained either on the basis of NH−NH NOEs, together with comparisons of chemical shifts and patterns of amide proton NOEs to those of the free protein (solid bars), or simply by chemical shift and NOE pattern comparisons (gray bars). For residues in bound B-MybR2R3 which could not be assigned on this basis, the minimum change in cumulative chemical shift occurring on DNA binding is shown (open bars).

the C-terminal regions of R2 (Q44−H50) and R3 (N94−T103) were estimated using the minimum change in chemical shift-based approach described above. This conservative method of analysis determines the minimum possible shifts for backbone amide signals induced by DNA binding and may give severe underestimates of the actual changes; however, it is still clear that signals from residues in these regions are strongly affected by DNA binding (Figure 7). It is perhaps worth noting that 12 of the unassigned backbone amide cross-peaks present in spectra of DNA-bound B-MybR2R3 were not attributed to a residue in the protein by the minimum change in chemical shift method, five of which are very low-field-shifted (Figure 6). Thus, DNA binding-induced chemical shift changes for some residues in the C-terminal regions of R2 and R3 are almost certainly much larger than those shown in Figure 7.

The chemical shift changes induced by DNA binding to B-MybR2R3 suggest that residues near the N termini and in helix 2 and helix 3 of both repeats are involved in DNA binding. However, the dramatic spectral changes seen

(Figures 6 and 7) probably reflect both direct interaction with the DNA and conformational changes in the protein, with one possibility being the formation of a stable helix at the C terminus of R2.

Conformational Heterogeneity in the B-MybR2R3−DNA Complex. In spectra of the B-MybR2R3−tom-1-A target site complex, backbone amide signals (^{15}N and ^{1}H) for a number of residues in R2, including V22, G26, T27, T31, L32, and H36, appear as doubled signals with a roughly 60:40 ratio for the two forms. Weak NH−NH exchange peaks are detectable between the two forms of T27 in 3D ^{15}N/^{1}H NOESY−HSQC spectra of the complex; however, the small differences in amide ^{1}H chemical shifts for the remaining residues prevent the observation of exchange peaks. Clearly, this data is an indication of the presence of at least two distinct forms of R2 in the B-MybR2R3−DNA complex in slow exchange on the NMR time scale.

Recently, two groups have reported the results of NMR studies of c-MybR2R3−DNA complexes (*25*−*27*, *44*). In a complex formed with a target site based on the mim-1-A Myb binding site (G**TAACGG**TCTAC), the imino proton resonances of base pairs 3, 4, 7, and 8 (with the core **TAACGG** sequence corresponding to base pairs 1−6) were found to be doubled with a roughly 60:40 intensity ratio, suggesting the presence of two different forms of the complex in slow exchange (*44*). These effects are strikingly similar to those seen for a number of the protein signals in spectra of B-MybR2R3 bound to the tom-1-A site (TCCT**TAACGG**ACTGAG). In contrast, studies of a complex formed between c-MybR2R3 and the Myb binding site from the enhancer region of SV40 (CC**TAACTG**ACACAT, MBS-1) reported no indication of two forms for the complex (*26*).

The Myb target site has been shown to be bipartite, with R3 interacting with the core AAC half-site and proposed to play the dominant role in sequence recognition, while R2 interacts with the more loosely defined second half-site (*45*, *46*). Recent mutational analysis of the Myb target site has revealed that the essential feature of the second half-site is the presence of at least one G in either position 5 or 6 and that X_5G_6-, G_5X_6-, and G_5G_6-containing sites all bind c-Myb very tightly (*47*). The essential tom-1-A and mim-1-A sites (see below) both have a G_5G_6 second half-site, so a likely explanation for the doubling of NMR signals in complexes formed with B-MybR2R3 and c-MybR2R3 is that R2 is able to interact favorably with either G_5 or G_6, respectively. This would also explain why only one form of the complex is seen for c-MybR2R3 bound to the MBS-1 target, which contains a T_5G_6 half-site and therefore can only make one type of interaction with R2.

A number of potential Myb-regulated vertebrate genes have now been identified; however, using stringent criteria, such as direct demonstration of the Myb inducibility of the endogenous gene, only a few of these, including *mim-1* and *tom-1*, have been unambiguously identified as Myb target genes (*22*, *23*). In the case of *tom-1*, it has been shown that only one of the two Myb binding sites (A) in the promoter is essential for Myb-mediated activation. Similarly, in the *mim-1* promoter, only the A and B sites appear to be important for regulation by Myb proteins (*22*). In light of the conformational heterogeneity observed in Myb−DNA complexes, it is interesting to note that all the functionally important Myb binding sites identified to date in promoters of bona fide Myb target genes contain a G_5G_6 second half-site, whereas the redundant sites are all X_5G_6. Thus, the second half-site of the Myb consensus sequence may play a more critical role in the control of gene expression by Myb proteins than previously thought, and the conformational flexibility identified in R2 may be important for this process through conformational heterogeneity of the DNA complex. This proposal is strongly supported by a very recent report by Brendeford and co-workers, which showed that an oncogenic variant of c-MybR2R3 containing three amino acid substitutions in R2 (equivalent to the AMV retroviral R2) was significantly more stable and folded, but the substitutions resulted in dramatically reduced stabilities for specific c-MybR2R3−DNA complexes and in reduced levels of transactivation of reporter genes in vivo (*48*).

ACKNOWLEDGMENT

We thank Dr. Andrew Lane for many useful discussions. The 600 MHz NMR spectra were recorded at the MRC Biomedical NMR Centre, National Institute for Medical Research, London, U.K.

REFERENCES

1. Cole, M. D. (1990) *Curr. Opin. Cell Biol. 2*, 502−508.
2. Lüscher, B., and Eisenman, R. N. (1990) *Genes Dev. 4*, 2235−2241.
3. Graf, T. (1992) *Curr. Opin. Genet. Dev. 2*, 249−255.
4. Thompson, M. A., and Ramsay, R. G. (1995) *BioEssays 17*, 341−350.
5. Golay, J., Basilico, L., Loffarelli, L., Songia, S., Broccoli, V., and Introna, M. (1996) *Int. J. Clin. Lab. Res. 26*, 24−32.
6. Lipsick, J. S. (1996) *Oncogene 13*, 223−235.
7. Nomura, N., Takahashi, M., Matsui, M., Ishii, S., Date, T., Sasamoto, S., and Ishizaki, R. (1988) *Nucleic Acids Res. 16*, 11075−11089.
8. Sitzmann, J., Nobentrauth, K., Kamano, H., and Klempnauer, K.-H. (1996) *Oncogene 12*, 1889−1894.
9. Trauth, K., Mutschler, B., Jenkins, N. A., Gilbert, D. J., Copeland, N. G., and Klempnauer, K.-H. (1994) *EMBO J. 13*, 5994−6005.
10. Toscani, A., Mettus, R. V., Coupland, R., Simpkins, H., Litvin, J., Orth, J., Hatton, K. S., and Reddy, E. P. (1997) *Nature 368*, 713−717.
11. Torelli, G., Selleri, L., Donelli, A., Ferrari, S., Emilia, G., Venturelli, D., Moretti, L., and Torelli, U. (1985) *Mol. Cell Biol. 5*, 2874−2877.
12. Robinson, C., Light, Y., Groves, R., Mann, D., Marais, R., and Watson, R. (1996) *Oncogene 12*, 1855−1864.
13. Sala, A., Kundu, M., Casella, I., Engelhard, A., Calabretta, B., Grasso, L., Paggi, M. G., Giordano, A., Watson, R. J., Khalili, K., and Peschle, C. (1997*) Proc. Natl. Acad. Sci. U.S.A. 94*, 532−536.
14. Ziebold, U., Bartsch, O., Marais, R., Ferrari, S., and Klempnauer, K.-H. (1997*) Curr. Biol. 7*, 253−260.
15. Klempnauer, K.-H., and Sippel, A. E. (1987) *EMBO J. 6*, 2719−2725.
16. Biedenkapp, H., Borgmeyer, U., Sippel, A. E., and Klempnauer, K.-H. (1988) *Nature 335*, 835−837.
17. Howe, K. M., Reakes, C. F. L., and Watson, R. J. (1990) *EMBO J. 9*, 161−169.
18. Oehler, T., Arnold, H., Biedenkapp, H., and Klempnauer, K.-H. (1990*) Nucleic Acids Res. 18*, 1703−1710.
19. Foos, G., Grimm, S., and Klempnauer, K.-H. (1992) *EMBO J. 11*, 4619−4629.
20. Dini, P. W., and Lipsick, J. S. (1993) *Mol. Cell. Biol. 13*, 7334−7348.
21. Weston, K. (1992) *Nucleic Acids Res. 20*, 3043−3049.
22. Ness, S. A., Marknell, A., and Graf, T. (1989) *Cell 59*, 1115−1125.

23. Burk, O., Worpenberg, S., Haenig, B., and Klempnauer, K.-H. (1997) *EMBO J. 16*, 1371−1380.
24. Carr, M. D., Wollborn, U., McIntosh, P. B., Frenkiel, T. A., McCormick, J. E., Bauer, C. J., Klempnauer, K.-H., and Feeney, J. (1996) *Eur. J. Biochem. 235*, 721−735.
25. Jamin, N., Gabrielsen, O. S., Gilles, N., Lirsac, P.-N., and Toma, F. (1993) *Eur. J. Biochem. 216*, 147−154.
26. Ogata, K., Morikawa, S., Nakamura, H., Sekikawa, A., Inoue, T., Kanai, H., Sarai, A., Ishii, S., and Nishimura, Y. (1994) *Cell 79*, 639−648.
27. Ogata, K., Morikawa, S., Nakamura, H., Hojo, H., Yoshimura, S., Zhang, R., Aimoto, S., Ametani, Y., Hirata, Z., Sarai, A., Ishii, S., and Nishimura Y. (1995*) Nat. Struct. Biol. 2*, 309−320.
28. Carr, M. D., and Mott, R. F. (1991) *FEBS Lett. 282*, 293−294.
29. Vuister, G. W., and Bax, A. (1993) *J. Am. Chem. Soc. 115*, 7772−7777.
30. Archer, S. J., Ikura, M., Torchia, D. A., and Bax, A. (1991) *J. Magn. Reson. 95*, 636−641.
31. Clore, G. M., Bax, A., Wingfield, P. T., and Gronenborn, A. M. (1990) *Biochemistry 29*, 5671−5676.
32. Norwood, T. J., Boyd, J., Heritage, J. E., Soffe, N., and Campbell, I. D. (1990) *J. Magn. Reson. 87*, 488−501.
33. Bax, A., Griffey, R. H., and Hawkins, B. L. (1983) *J. Am. Chem. Soc. 105*, 7188−7190.
34. Sklenar, V., Piotto, M., Leppik, R., and Saudek, V. (1993) *J. Magn. Reson. 102*, 241−245.
35. Press, W. H., Flannery, B. P., Teukolsky, S. A., and Vetterling, W. T. (1988*) Numerical Recipes in C, The Art of Scientific Computing*, Cambridge University Press, Cambridge, U.K.
36. Bartels, C., Xia, T., Billeter, M., Güntert, P., and Wüthrich, K. (1995) *J. Biomol. NMR 5*, 1−10.
37. Wüthrich, K. (1986) *NMR of Proteins and Nucleic Acids*, Wiley, New York.
38. Güntert, P., and Wüthrich, K. (1991) *J. Biomol. NMR 1*, 447−456.
39. Güntert, P., Braun, W., and Wüthrich, K. (1991) *J. Mol. Biol. 217*, 517−530.
40. Güntert, P., Berndt, K. D., and Wüthrich, K. (1993) *J. Biomol. NMR 3*, 601−606.
41. Koradi, R., Billeter, M., and Wüthrich, K. (1996) *J. Mol. Graphics 14*, 51−55.
42. Güntert, P., Mumenthaler, C., and Wüthrich, K. (1997) *J. Mol. Biol. 273*, 283−298.
43. Farmer, B. T., Constantine, K. L., Goldfarb, V., Friedrichs, M. S., Wittekind, M., Yanchunas, J., Robertson, J. G., and Müller, L. (1996) *Nat. Struct. Biol. 3*, 995−997.
44. Jamin, N., Le Tilly, V., Zargarian, L., Bostad, A., Besancon-Yoshpe, I., Lirsac, P.-N., Gabrielsen, O. S., and Toma, F. (1996) *Int. J. Quantum Chem. 59*, 333−341.
45. Ording, E., Kvavik, W., Bostad, A., and Gabrielsen, O. S. (1994) *Eur. J. Biochem. 222*, 113−120.
46. Tanikawa, J., Yasukawa, T., Enari, M., Ogata, K., Nishimura, Y., Ishii, S., and Sarai, A. (1993) *Proc. Natl. Acad. Sci. U.S.A. 90*, 9320−9324.
47. Ording, E., Bergholtz, S., Brendeford, E. M., Jamin, N., and Gabrielsen, O. S. (1996) *Oncogene 13*, 1043−1051.
48. Brendeford, E. M., Myrset, A. H., Hegvold, A. B., Lundin, M., and Gabrielsen, O. S. (1997) *J. Biol. Chem. 272*, 4436−4443.

BI972861Z